

Tailoring of uniaxial magnetic anisotropy in Permalloy thin films using nanorippled Si substrates

Sarathlal Koyiloth Vayalil¹ , Aswathi Koorikkat¹, Ajesh K Gopi¹,
Stephan V Roth² and P S Anil Kumar¹

¹ Department of Physics, Indian Institute of Science, Bangalore, 560012, India

² Deutsches Elektronen-Synchrotron (DESY), D-22607 Hamburg, Germany

E-mail: sarathlal@iisc.ac.in

Received 5 August 2019, revised 9 December 2019

Accepted for publication 17 January 2020

Published 6 February 2020



Abstract

In this work the investigation of in-plane uniaxial magnetic anisotropy induced by the morphology due to ion beam erosion of Si(1 0 0) has been done. Ion beam erosion at an oblique angle of incidence generates a well-ordered nanoripple structure on the Si surface and ripple propagates in a direction normal to ion beam erosion. Permalloy thin films grown on such periodic nanopatterns show a strong uniaxial magnetic anisotropy with easy axis of magnetization in a direction normal to the ripple wave vector. The strength of uniaxial magnetic anisotropy is found to be high for the low value of ripple wavelength; it is decreasing with increasing value of ripple wavelength. Similarly, the strength of uniaxial magnetic anisotropy decreases with increasing Permalloy film thickness. Grazing incidence small angle x-ray scattering data reveals an anisotropic growth of Permalloy thin films with preferential orientation of grains in the direction normal to the ripple wave vector. Permalloy thin film growth is highly conformal with the film surface replicating the substrate ripple morphology up to a film thickness of 50 nm has been observed. Correlation between observed uniaxial magnetic anisotropy to surface modification has been addressed.

Keywords: ion beam erosion, nanoripples, grazing incidence small angle x ray scattering, magnetic thin films, magnetic anisotropy

(Some figures may appear in colour only in the online journal)

1. Introduction

Nanostructuring by low energy ion beams gained significant relevance in recent years because of its simplicity, versatility and cost-effectiveness to produce well-ordered nanopatterns over a large area (several tens of cm²). Over the past decade, an abundance of experimental and theoretical work has been established on the effect of different experimental parameters on ion beam induced pattern formation as well as the mechanism of formation [1–18]. Depending on the sputtering parameters like ion species, ion incidence angle, ion beam energy, ion flux, fluence, different nanoscale patterns can be formed such as wave-like periodic nanoripple patterns [4–13], or hexagonally ordered dots [1–3] or holes [14, 15], having

periodicity varying from a few tens to hundreds of nanometers. These patterns can be produced on different materials, crystalline or amorphous materials, including metals and polymers. In general, ripple-like structures are found to be formed, when a flat surface of any elemental solid is bombarded with ions at an oblique angle of incidence. Bradley and Harper had given the first satisfactory theoretical explanation by considering the competition between surface instability caused by the curvature dependent sputtering and surface relaxation mechanism [16].

Nanoripple substrates have been used widely as a template to grow thin films and multilayers to tailor functional properties in a controlled manner. Self-organized metallic nanoparticles and nanowire arrays have been produced by depositing

metal films on such rippled templates. Tunable plasmonic [19–22], as well as anisotropic magnetic properties [23–29] have been observed in metallic thin films grown on periodic nanorippled templates. A recent article highlighted a different technological use of nanorippled Ge substrates as a bio-active surface by employing multi scale preparation processes along with ion beam implantation for regenerative applications [30]. Surface and interface roughness or modulations play an important role in many properties of magnetic thin films. Also, it has been theoretically predicted that dipolar interaction and surface curvature can produce perpendicular anisotropy which can be controlled by engineering special types of periodic surface structures [31]. Bisio *et al* used ion beam erosion to get step induced uniaxial magnetic anisotropy (UMA) in Fe thin films on flat Ag(001) substrates [32]. Liedke *et al* tuned the UMA of ferromagnetic thin films by growing on nano rippled templates of different materials prepared by ion beam erosion. The competition between biaxial and UMA have been observed in thickness dependent studies of Fe thin film grown epitaxially on ripple patterned MgO(001) templates [27]. In our earlier studies, we did a detailed growth analysis of Co thin film on nano rippled Si using *in situ* MOKE and resistivity studies [23, 24].

In this work, we report on the tailoring and tuning of the uniaxial magnetic anisotropy of one of the potentially relevant soft magnetic materials, Permalloy (Py) thin films deposited on nano rippled Si substrates prepared by low energy Ar⁺ ion beam erosion. The magnetic anisotropy of soft magnetic thin films is one of the most important properties determining the sensor function of magneto-resistive sensors in magnetoelectronic applications. In this work, we correlated the influence of ripple wavelength of the Si substrate as well as the thickness of Py films with the observed strong UMA.

2. Experimental details

Nanorippled Si(100) substrates have been prepared by low energy ion beam erosion and details of the preparation have been mentioned elsewhere [6, 33]. Nanorippled Si substrates with different periodicity values ranging from 24 nm to 60 nm by tuning the Ar⁺ ion beam energy from 300 eV to 800 eV have been used for the deposition of Py thin films. Polycrystalline Py films were grown at normal incidence on such templates by DC sputtering from a 2-inch diameter magnetron source in the argon pressure range of 5×10^{-3} millibars. Thickness was measured *in situ* using a quartz crystal thickness monitor, which has been calibrated initially against the thickness value obtained from the *ex situ* x-ray reflectivity (XRR) measurements. Base pressure in the deposition chamber was 4×10^{-8} mbar. During Py deposition, the substrate has been rotated to avoid any geometrical effects. The deposition rate of Py film was maintained at 0.04 nm s^{-1} . All Py films were coated with 2 nm thick Pt film to avoid oxidation. Thickness and roughness of the films were calculated using XRR techniques.

Surface morphology of the rippled substrate and deposited Py films of different thicknesses were analyzed by means of atomic force microscopy (AFM) in tapping mode

(Dimension Icon Atomic Force Microscope from Bruker). Fast Fourier transform (FFT) of the AFM image was done using the software WSxM [34]. Further detailed morphological characterization of the sample has been performed using grazing-incidence small-angle x-ray scattering with a micro-beam (μ GISAXS) from MiNaXS/P03 beamline (PETRA III, DESY) [35]. Photon energy of 12.85 keV (X-ray wavelength $\lambda = 0.0965 \pm 0.0002 \text{ nm}$) with a beam size of $(22 \times 10 \text{ }\mu\text{m})$ at the sample position was used. The sample-to-detector distance was set at $3080 \pm 1 \text{ mm}$ and PILATUS 1M (Dectris Ltd., Switzerland) with a pixel size of $(172 \times 172 \text{ }\mu\text{m}^2)$ was used as the detector. The μ GISAXS data have been extracted using DPDAK program [36]. Magneto-optical Kerr effect (MOKE) has been used to study the magnetic properties. MOKE measurements were done in longitudinal geometry using He–Ne laser. Angular dependence of the magnetization was studied by rotating the sample holder azimuthally around its normal axis. In order to extract quantitative magnetization information SQUID-VSM technique has also been employed.

3. Results and discussion

As mentioned in the experimental part, nanorippled Si substrates prepared by low energy ion beam erosion have been used as templates to grow modulated thin films with higher ordering. A detailed morphological studies on the dependence of ion beam parameters on pattern formation has been studied earlier [6]. We have employed rippled templates having different wavelength values ranging from 24 nm to 59 nm for growing Py films. The different wavelength samples have been prepared by tuning the ion energy by keeping the other parameters like ion incidence angle, ion flux etc constant. A detailed ion energy dependence on ripple wavelength has been done by many groups [11, 33]. Figures 1(a)–(c) show AFM images of Py films (thickness, $t = 15 \text{ nm}$) deposited on nano rippled Si substrates with selected wavelength values ($\Lambda \sim 24 \text{ nm}, 48 \text{ nm}, 59 \text{ nm}$). Pronounced ripple patterns are visible for Py films deposited on all selected wavelengths range.

The insets of figure 1 show the two-dimensional fast Fourier transform (2D-FFT) images of the corresponding real space images. The dominant spatial frequencies present on the sample surface can be extracted by FFT. The two intense symmetrical lobes located about the high-intensity zero-frequency signal shows the presence of anisotropic ripple patterned film surfaces. More number of lobes indicating the higher ordering of the patterned films. Line cuts made along the FFT images are plotted respectively in (d)–(f). Periodicity/ wavelength of the ripples can be estimated by measuring the side peak position using the expression $\Lambda = 1/\text{Spatial frequency}(X)$.

For a statistical morphological analysis surface sensitive μ GISAXS measurements have been carried out. μ GISAXS is an advanced technique to probe surface, interface and buried structures in thin films due to its surface sensitivity [37–39]. It is a non-destructive and contact-free measurement of sample structures with feature sizes between 1 nm and $1 \text{ }\mu\text{m}$, yielding statistical information of the whole illuminated

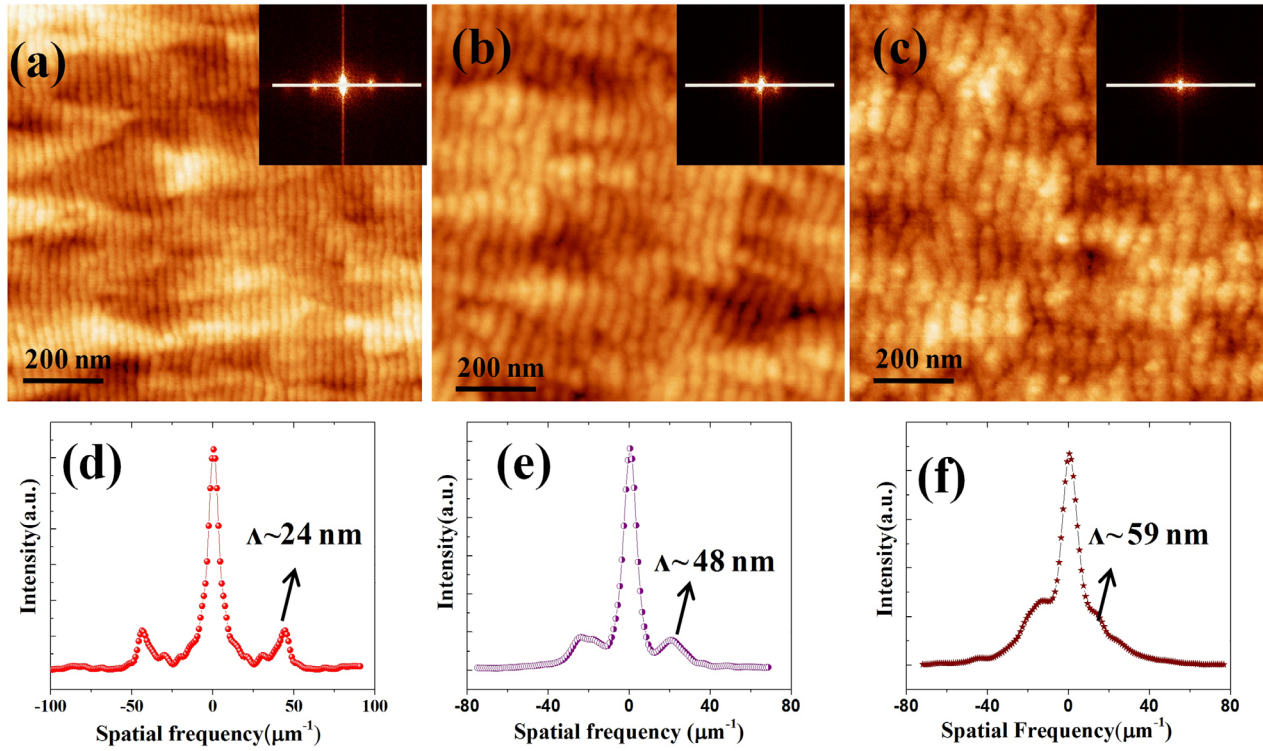


Figure 1. AFM topographic images of Py thin film ($t = 15$ nm) deposited on nano rippled Si substrates having different wavelength values, $\Lambda \sim$ (a) 24 nm (b) 48 nm and (c) 59 nm with corresponding FFT images as insets. Line cuts (white line) made along the FFT images are shown in (d)–(f).

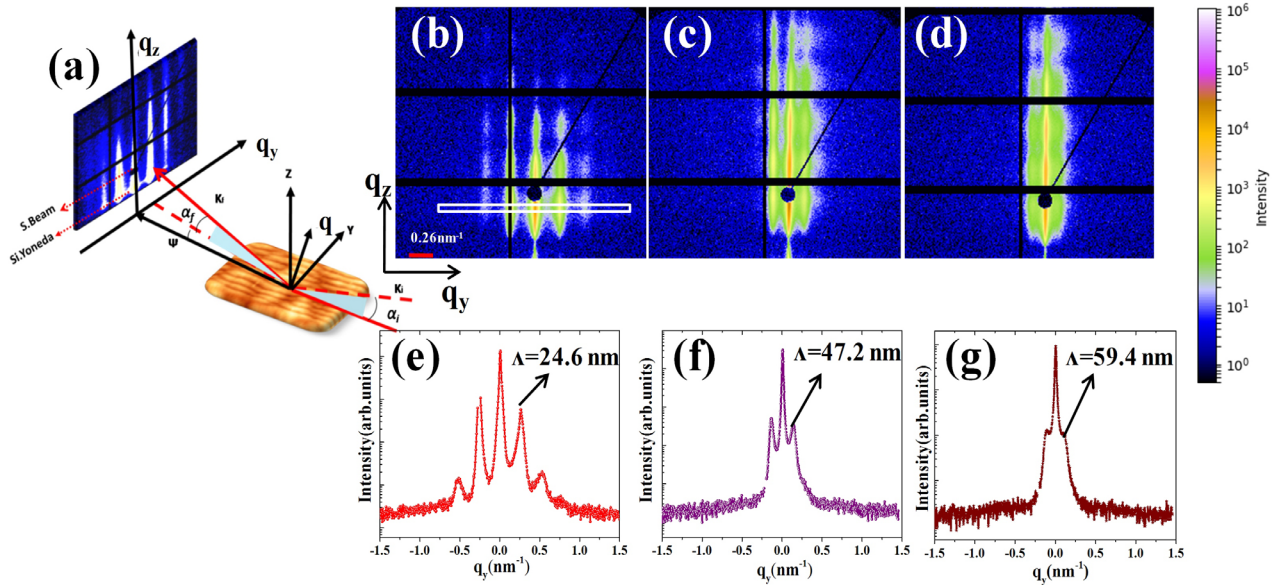


Figure 2. (a) shows the schematic of the GISAXS measurements geometry. (b)–(d) represent the two-dimensional μ GISAXS images of Py thin film ($t = 15$ nm) deposited on nanorippled Si substrates having different wavelength values measured at an incident angle 0.4° . Corresponding line-cuts made along the horizontal direction (see the white box drawn in (b)), along q_y for a fixed value of q_z value (around Si Yoneda peaks) are shown in (e)–(g).

sample volume. The schematic of the scattering geometry of the μ GISAXS measurement is depicted in figure 2(a). The x, z plane defines the incident x-ray beam and z -axis is always taken to be normal to the sample surface. \vec{k}_i and \vec{k}_f represent the incident and scattered wave vectors respectively. The components (q_x , q_y and q_z) of the scattering momentum

transfer $\vec{Q} = \vec{k}_f - \vec{k}_i$ are defined by the incident and scattering angles α_i , α_f and in-plane angle ψ . In this geometry, the x-ray beam incident on the sample at an angle α_i is close to the critical angle of the sample (typically $\leq 1^\circ$) to undergo total external reflection and enhances the surface sensitivity. The beam is then scattered specularly and diffusely. The scattered,

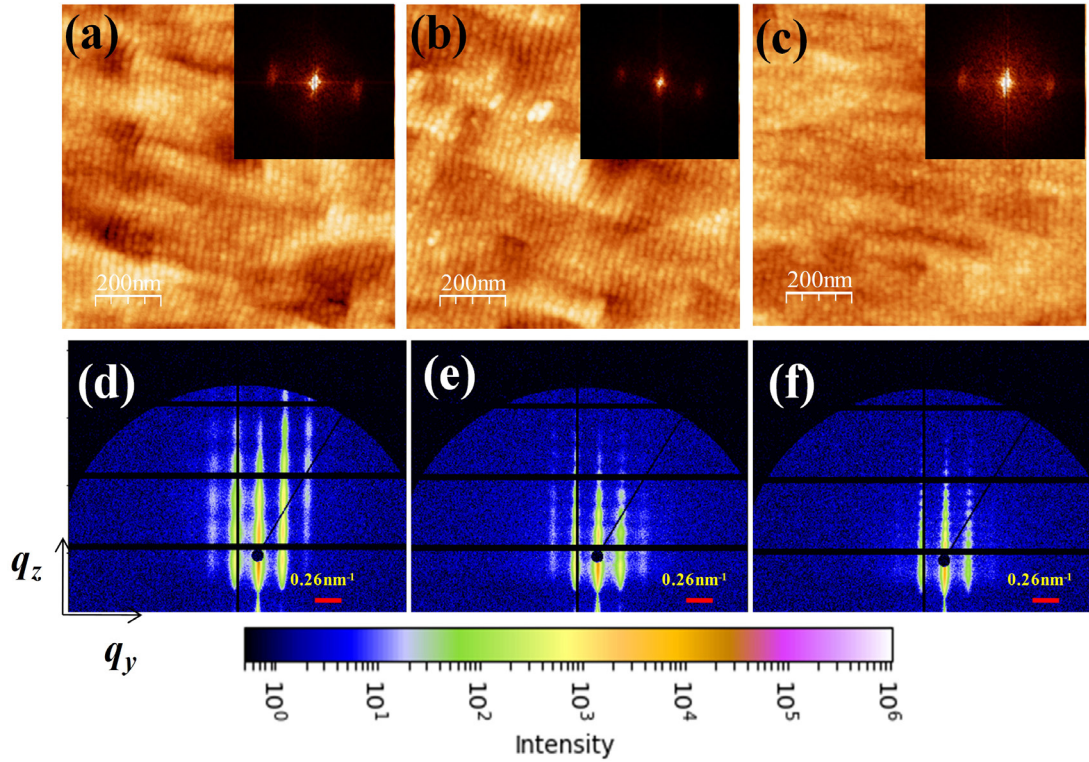


Figure 3. AFM images of Py films having different thickness values $t = 8$ nm, 25 nm and 50 nm deposited on $\Lambda = 24$ nm rippled Si substrates are shown in figures 2(a)–(c) respectively. Corresponding FFT images are shown in the insets. Figures 2(d)–(f) are the 2D GISAXS plots of $t = 8$ nm, 25 nm and 50 nm respectively.

detected intensity is related to the electron density differences present in the system. The measurements have been performed with incident x-ray beams normal to the ripple wave vector \mathbf{k} . The samples have been rotated in azimuthal direction in small steps of 1 degree up to ten degrees in both the directions to align the x-ray beam exactly in a direction normal to the ripple wave vector, in order to avoid any kind of asymmetry in the GISAXS pattern due to misalignment of x ray beam with ripple direction.

Figures 2(b)–(d) show the two-dimensional μ GISAXS images measured at an incident angle 0.4° corresponding to different wavelength values. The footprint calculation for the x ray beam ($22 \times 10 \mu\text{m}$) shows that, it is sufficiently less for the sample size used ($6\text{mm} \times 6\text{mm}$) for all our measurements under the given incident angle. The periodic ripple pattern is confirmed by the presence of clearly separated side streaks in the two-dimensional GISAXS map displayed in figures 2(b)–(d). Peaks on each side of the specular peak indicate the correlated structure formation on the samples. Line-cuts made along the horizontal direction, along q_y for a fixed value of q_z value (around Si Yoneda peaks) are shown in figures 2(e)–(g). The structures are separated by a real space distance of $\xi = 2\pi/q_y$. The wavelength values obtained from peak positions are 24.6 nm, 47.2 nm and 59.4 nm. The wavelength values obtained from GISAXS have been used in the further calculations. More number of side peaks in GISAXS images indicating the presence of higher ordering the samples. Also peak width full width half maximum (FWHM) is related to the correlation length as $1/\text{FWHM}$. $\Lambda = 24.6$ nm sample is found to be highly ordered as compared to the other

wavelengths samples that we have prepared. An asymmetry in the intensity distribution with respect to $q_y = 0\text{nm}^{-1}$ is also observed, which reveals that the morphology of the ripple surface is not symmetric [4]. The low intensity side streaks are corresponding to the steeper slope of the ripple structures. The observed asymmetry is found to be reversed for the measurement done after rotating the sample 180 degree in azimuthal direction with respect to the x-ray beam.

Py thin films deposited on $\Lambda = 24.6$ nm Si rippled substrates have been chosen for thickness dependent studies. AFM images of selected Py films with different thickness values ($t = 10$ nm, 25 nm, 50 nm) deposited on $\Lambda = 24.6$ nm is shown in figures 3(a)–(c). Corresponding FFT images are shown in insets. We observe that a rippled surface morphology of the Py films is even visible for very high thickness value of 50 nm.

Figures 3(d)–(f) show the two-dimensional μ GISAXS images measured at an incident angle 0.4° corresponding to different thickness values. Interference fringes both in central and on the side peaks along q_z direction imply the high correlation between the Py film and the ripple surface. Line-cut made along the horizontal direction, along q_y for a fixed value of q_z and vertical cuts made along side bands corresponding to fixed q_z value along q_z direction are shown in figures 4(a) and (b) respectively. One of the 2D μ GISAXS images has been selected to represent the direction of line cuts made. The side peak position is constant for all thickness values studied indicating that the ripple wavelength value of the substrate determines the ripple wavelength for the deposited Py films. Additionally, the presence of higher order peaks for higher

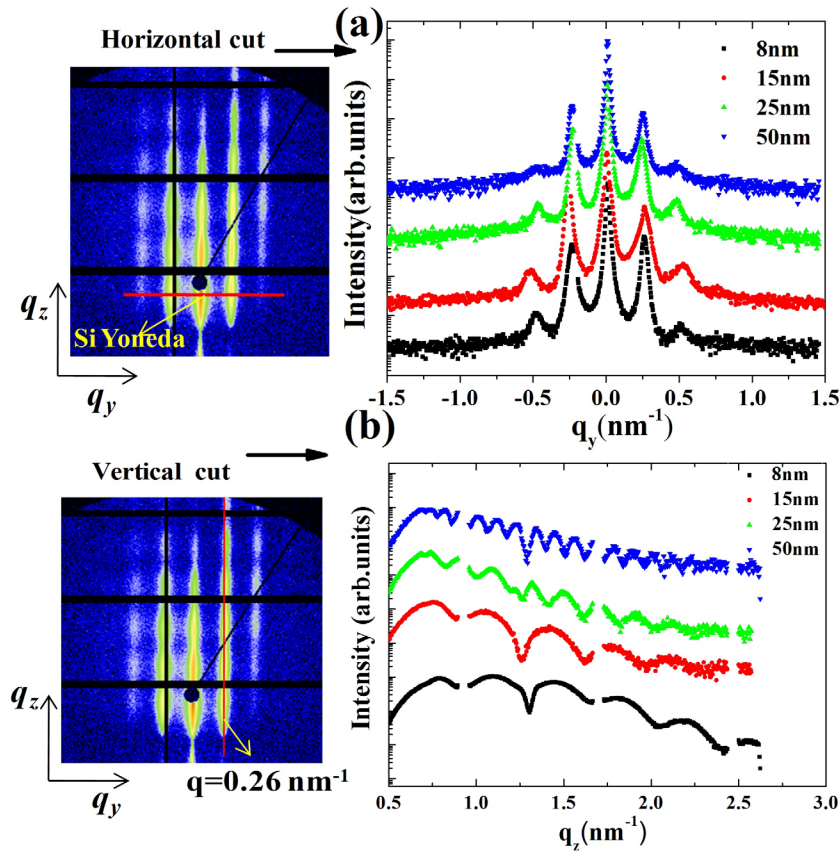


Figure 4. (a) shows horizontal cuts along q_y around Si Yoneda peak region of the 2D GISAXS data for different Py thickness values (shifted along the intensity axis) and (b) shows the vertical cut along q_z direction for a chosen value of $q_y = 0.26 \text{ nm}^{-1}$. One of the 2D GISAXS images has been selected to represent the direction of line integrals made.

thickness values shows that the Py film is highly ordered and replicating the morphology up to large extent. The interference stemming from the correlated film thickness can be seen along q_z direction with damped intensity oscillations. The damping of the oscillations is a measure of the correlation between the rippled substrate and the film at this spatial frequency. Strong decay in intensity corresponds to low conformity with the film. In our case even for a 50nm thick Py film, the fringes are clearly visible for higher q_z values as well as damping of oscillations are not high indicating the extent of correlation for large film thickness values even for $\sim 1.4 \text{ nm}$ depth rippled Si substrates.

To study the magnetic properties of Py film grown on nano rippled Si samples magnetic hysteresis data $M(H)$ were collected using longitudinal MOKE measurements. For comparison, we also checked the $M(H)$ data for a flat Py film (15 nm) deposited on a pristine cleaned Si(100) substrate. This Py film had a small coercivity of approximately 1 Oe, and did not show any direction dependence within the film plane, implying that Py films on pristine Si substrates are magnetically isotropic (not shown). Figure 5(a) show the normalized magnetic hysteresis data with applied field (i) along the ripple wave vector \mathbf{k} (open circles) and (ii) normal to \mathbf{k} (filled circles) for five different ripple wavelengths ($\Lambda = 24.6 \text{ nm}$, 35.2 nm , 47.2 nm , 52.6 nm , 59.4 nm). Corresponding polar plots of remanent magnetization M_r normalized by the saturation magnetization M_s with the change of the in-plane angle ϕ with $\phi = 0$

representing the field direction along \mathbf{k} is shown in figure 5(b). From these graphs it is clear that the Py films deposited on nanorippled Si substrates are exhibiting well defined uniaxial magnetic anisotropy (UMA); direction normal to the ripple wave vector \mathbf{k} is the easy axis whereas direction parallel to \mathbf{k} corresponds to hard axis. Strong uniaxial magnetic anisotropy is observed for the case of $\Lambda = 24.6 \text{ nm}$ ripples and strength of UMA is found to be decreasing with increasing wavelength. For more quantitative analysis, SQUID-VSM measurements on the same samples have been undertaken. It can be seen that the saturation field, i.e. the applied magnetic field at which the magnetic moments align completely in the direction of the field, strongly depends upon the ripple wavelength magnitudes. Saturation magnetic field is found to be increased from $\sim 15 \text{ Oe}$ to $\sim 100 \text{ Oe}$ as Λ decreased from 59.4 nm to 24.6 nm . The value of magnetic anisotropy energy K was calculated using the relation of $M_s H_a / 2$, where H_a is the anisotropy field and M_s is the saturation magnetization. The dependence of ripple wavelength on magnetic anisotropy energy is shown in figure 5(c). Strong dependence on Λ has been observed for low wavelength regime (24 nm – 48 nm) and for larger Λ (above 48 nm) the magnetic anisotropy energy value decreases only slightly.

For the thickness dependent magnetic anisotropy studies, Py films deposited on $\Lambda = 24.6 \text{ nm}$ ripple sample showing strongest UMA has been chosen. Figure 6(a) shows the magnetization loop measured along and normal to the ripples and

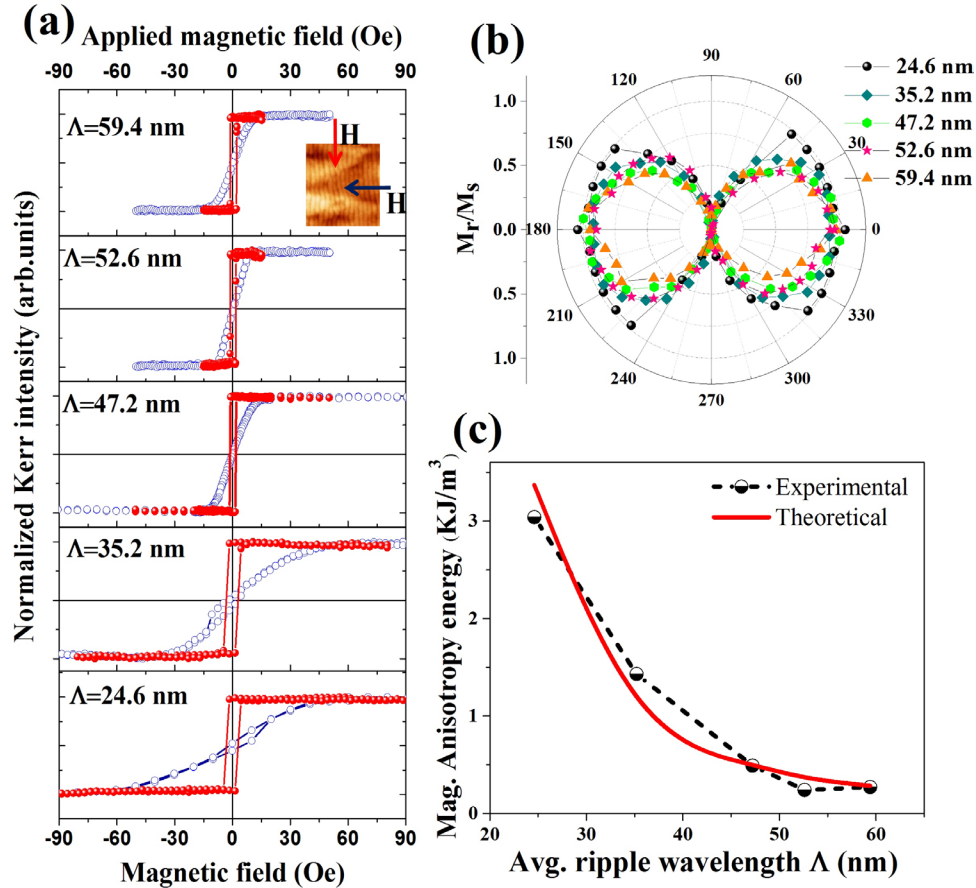


Figure 5. (a) show the normalized magnetic hysteresis data with applied field (i) along the \mathbf{k} (blue open circles) and (ii) normal to \mathbf{k} (red filled circles) for Py films deposited nanorippled Si having different ripple wavelengths ($\Lambda = 24.6$ nm, 35.2 nm, 47.2 nm, 52.6 nm, 59.4 nm). Corresponding polar plots of remanent magnetization M_r normalized by the saturation magnetization M_s with the change of the in-plane angle ϕ with $\phi = 0$ representing the field direction normal \mathbf{k} is shown in (b). Variation of magnetic anisotropy energy (measured from VSM data) with increasing values of ripple wavelength is shown in (c). Red curve in (c) indicates the simulated data using Schlömann's formula.

corresponding polar plots of remanent magnetization M_r normalized by the saturation magnetization M_s with the change of the in-plane angle ϕ with $\phi = 0$ representing the field direction along \mathbf{k} is shown in figure 6(b). Strong uniaxial magnetic anisotropy has been observed in the case of low thickness value 8 nm Py film with easy axis of magnetization in a direction normal to \mathbf{k} . Saturation field value is found to be decreased from ~ 140 Oe to ~ 30 Oe as thickness is increased from 8 nm to 50 nm. From the qualitative data analysis of magnetic anisotropy energy calculation using SQUID-VSM data for different thickness values, the anisotropy energy is found to be gradually decreasing with increasing value of Py film thickness and the corresponding plot is shown in figure 6(c).

It is clear from recent report that, in the case of large ripple amplitude and small film thickness values, the magnetization perfectly follows the surface profile and magnetic anisotropy has only volume contribution, with no contribution from possible stray dipolar fields [26]. So we can neglect the volume contribution to the observed uniaxial magnetic anisotropy. In our case of small ripple amplitude and large film thickness, all the spins get aligned parallel to each other and the anisotropy has its origin mainly due to the dipolar stray fields generated at the surface/interface. As per the studies reported, additional contribution to the magnetic anisotropy can come also due to

epitaxy with the substrate [27, 40], and/or the surface edge/steps induced anisotropy [32] in addition to the shape induced anisotropy if the substrate is single crystalline. Ion beam erosion results in the formation of a very thin (~ 2 nm) amorphous Silicon dioxide layer at the surface and it has been observed while fitting XRR curve as well as in our earlier studies on the ripple formation [24]. Since the surface of the rippled samples are amorphous in nature, possibility of epitaxy or edge/steps anisotropy can be excluded in our case.

Schlömann's theory [41] for demagnetization field in thin magnetic films due to rough surface, $K_{\text{dip}} = 2\pi M_s^2 \omega_{\text{rms}}^2 / \Lambda D$, where Λ represents the ripple wavelength, M_s the saturation magnetization, ω_{rms} the surface modulation amplitude and D the ferromagnetic film thickness, has been used to explain the observed nature of wavelength and the thickness dependence of K . This theory makes the assumption that the magnetization is to be strictly oriented in in-plane direction; no local variation in magnetization direction is added. In our case the decrease of UMA with Λ shows a strong decay of dipolar interactions with increasing Λ .

Since in Λ dependence of K study, thickness of the Py film was kept constant, and it will ensure a constant M_s value for all samples. So it is important to analyze the variation of average roughness, ω_{rms} for different Λ samples. The

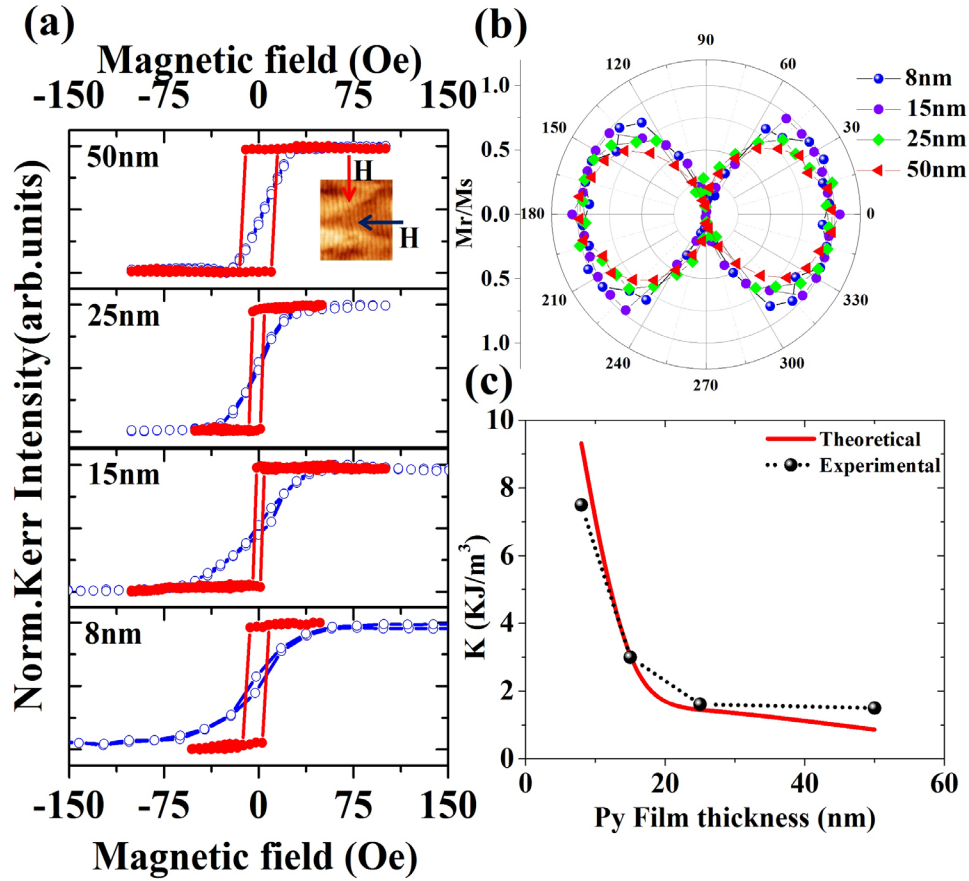


Figure 6. (a) show the normalized magnetic hysteresis data with applied field (i) along the k (blue open circles) and (ii) normal to k (red filled circles) for Py films of different thickness values deposited on nano rippled Si having ripple wavelength $\Lambda = 24$ nm. Corresponding polar plots of remanent magnetization M_r , normalized by the saturation magnetization M_s with the change of the in plane angle ϕ with $\phi = 0$ representing the field direction normal to k is shown in figure (b). Variation of magnetic anisotropy energy (measured from VSM data) with increasing values of Py film thickness is shown in (c). Red curve in (c) indicates the simulated data using Schlömann's formula.

corresponding variation calculated from x-ray reflectivity data is shown in figure 7 as ω_{rms}^2 versus Λ . Average roughness is found to be a decreasing non monotonously with increasing Λ values. In thickness dependence data also, we have observed a decreasing tendency of average roughness with increasing film thickness values. Overall magnetic anisotropic energy will decrease with increasing value of Λ as well as increasing film thickness. Calculated magnetic anisotropy energy values based on Schlömann's formula for different wavelength values and thickness values are also plotted in Figures 5(c) and 6(c) respectively. We have observed some disagreement of the experimental data with the calculated values. This discrepancy can be due to the following facts. The actual surface profile of the film is found to be deviated from an ideal sinusoidal contour due to various defects like height corrugations, overlapping ripples, pattern dislocations etc. Also other high frequency roughness terms originated due to the stochastic nature of the thin film growth, which in general is found to increase with film thickness, would also contribute to the UMA [42, 43].

In conclusion, we have employed nanorippled Si substrates prepared by low energy ion beam erosion to tailor uniaxial magnetic anisotropy of Py films deposited on it. Grazing incidence small angle x-ray scattering data reveals an anisotropic

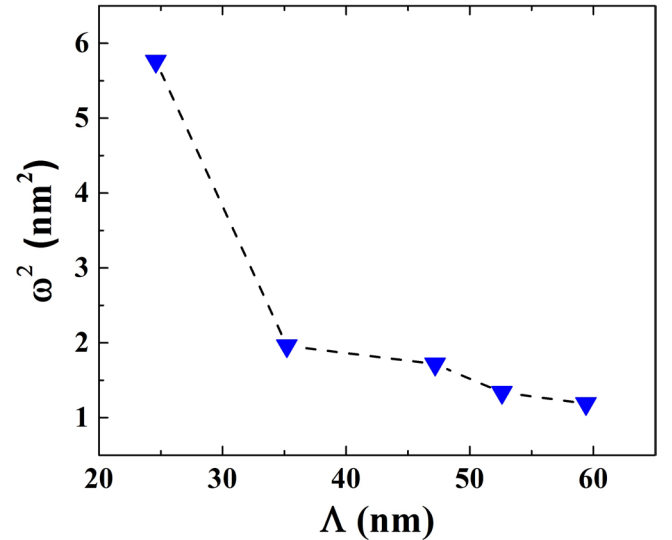


Figure 7. Variation of average roughness with increasing value of ripple wavelength for 15 nm thick Py films.

growth of Py thin films with preferential orientation of grains in the direction normal to the ripple wave vector. Py thin film growth is highly conformal with the film surface replicating the substrate ripple morphology up to a film thickness

of 50 nm has been observed. The strength of uniaxial magnetic anisotropy is found to be high for the low value of ripple wavelength and it is decreasing with increasing value of ripple wavelength. Similarly, the strength of uniaxial magnetic anisotropy decreases with increasing Permalloy film thickness values. Tuning of magnetic anisotropy of soft magnetic thin film is having potential applications in magneto resistive sensors. This method of growing soft magnetic thin films on large area nanopatterned templates prepared by low energy ion beam erosion with the wide possibility of tunable nanostructure parameters will open up new dimensions in applications which are using patterned soft magnetic thin films.

Acknowledgments

SKV is thankful to the Department of Science and Technology, New Delhi, India for DST-INSPIRE Faculty fellowship. Portions of this research work were carried out at the light source PETRA III, DESY, a member of the Helmholtz Association (HGF). We would like to thank Dr Matthias Schwarzkopf and Dr Pallavi Pandit for assistance at the beamline P03, PETRA III, DESY. Thankful to A Keller and S Facsko, Helmholtz-Zentrum Dresden-Rossendorf for helping in rippled template preparation. Financial support by the Department of Science and Technology (Government of India) provided within the framework of the India @DESY collaboration is gratefully acknowledged.

ORCID iDs

Sarathlal Koyiloth Vayalil  <https://orcid.org/0000-0003-3483-3310>

References

- [1] Facsko S, Dekorsy T, Koerdts C, Trappe C, Kurz H, Vogt A and Hartnagel H L 1999 *Science* **285** 1551–3
- [2] Brown A D and Erlebacher J 2005 *Phys. Rev. B* **72** 075350
- [3] Ou X, Keller A, Helm M, Fassbender J and Facsko S 2013 *Rev. Lett.* **111** 016101
- [4] Babonneau D, Vandenhecke E and Camelio S 2017 *Phys. Rev. B* **95** 085412
- [5] Koyiloth Vayalil S, Gupta A, Roth S and Ganesan V 2015 *J. Appl. Phys.* **117** 024309
- [6] Koyiloth Vayalil S, Potdar S, Gangrade M, Ganesan V and Gupta A 2013 *Adv. Mat. Lett.* **4** 398–401
- [7] Koyiloth Vayalil S, Gupta A and Roth S 2017 *Appl. Phys. A* **123** 225
- [8] Headrick R and Zhou H 2009 *J. Phys.: Condens. Matter* **21** 224005
- [9] Erlebacher A M J 1999 *Phys. Rev. Lett.* **82** 2330–3
- [10] Frost F and Rauschenbach B 2003 *Appl. Phys. A: Mater. Sci. Process* **77** 1–9
- [11] Ziberi B, Frost F, Höche T and Rauschenbach B 2005 *Appl. Phys. Lett.* **92** 063102
- [12] Zhang K, Brötzmann M and Hofäss H 2011 *New. J. Phys.* **13** 013033
- [13] El-Atwani O, Gonderman S, DeMasi A, Suslova A, Fowler J, El-Atwani M, Ludwig K and Allain J P 2013 *J. Appl. Phys.* **113** 124305
- [14] Wei Q, Zhou X, Joshi B, Chen Y, Li K D, Wei Q, Sun K and Wang L 2009 *Adv. Mater.* **21** 2865–9
- [15] Kahng B, Jeong H and Barabási A L 2001 *Appl. Phys. Lett.* **78** 805
- [16] Bradley R and Harper M 1988 *J. Vac. Sci. Technol. A* **6** 2390
- [17] Cuerno R and Barabási A L 1995 *Phys. Rev. Lett.* **74** 4746
- [18] Rusponi S, Boragno C and Valbusa U 1997 *Phys. Rev. Lett.* **78** 2795
- [19] Oates T W H, Keller A, Facsko S and Mücklich A 2007 *Plasmonics* **2** 47–50
- [20] Camelio S, Vandenhecke E, Rousselet S and Babonneau D 2014 *Nanotechnology* **25** 035706
- [21] Babonneau D, Camelio S, Simonot L, Pailloux F, Guerin P, Lamongie B and Lyon O 2011 *Europhys. Lett.* **93** 26005
- [22] Ranjan M, Oates T W H, Facsko S and Müller W 2010 *Opt. Lett.* **35** 2576–8
- [23] Koyiloth Vayalil S, Kumar D and Gupta A 2011 *Appl. Phys. Lett.* **98** 123111
- [24] Koyiloth Vayalil S, Kumar D, Ganesan V and Gupta A 2012 *Appl. Surf. Sci.* **258** 4116
- [25] Arranz M A, Colino J M and Palomares F J 2014 *J. Appl. Phys.* **115** 183906
- [26] Chen K, Frömter R, Rössler S, Mikuszeit N and Oepen H P 2012 *Phys. Rev. B* **86** 064432
- [27] Liedke M, Kröner M, Lenz K, Grossmann F, Facsko S and Fassbender J 2012 *Appl. Phys. Lett.* **100** 242405
- [28] Körner M, Lenz K, Gallardo R A, Fritzsche M, Mücklich A, Facsko S, Lindner J, Landeros P and Fassbender J 2013 *Phys. Rev. B* **88** 054405
- [29] Büttner F, Zhang K, Seyffarth S, Liese T, Krebs H U, Vaz C and Hofäss H 2011 *Phys. Rev. B* **84** 064427
- [30] Dell'Anna R, Masciullo C, Iacob E and Barozzi M 2017 *RSC Adv.* **7** 9024
- [31] Tretiakov O A, Morini M, Vasylykevych S and Slastikov V 2017 *Phys. Rev. Lett.* **119** 077203
- [32] Bisio F, Moroni R, Buatier de Mongeot F, Canepa M and Mattera L 2006 *Phys. Rev. Lett.* **96** 057204
- [33] Keller A, Facsko S and Möller W 2009 *J. Phys.: Condens. Matter* **21** 495305
- [34] Horcas I, Fernández R, Gómez-Rodríguez J, Colchero J, Gómez-Herrero J and Baro A 2007 *Rev. Sci. Instrum.* **78** 013705
- [35] Buffet A et al 2012 *J. Synchrotron Radiat.* **19** 647–53
- [36] Benecke G et al 2014 *J. Appl. Cryst.* **47** 1797–803
- [37] Roth S V 2016 *J. Phys.: Condens. Matter* **28** 403003
- [38] Roth S V et al 2015 *J. Appl. Cryst.* **48** 1827
- [39] Hexemer A and Müller-Buschbaum P 2015 *IUCr* **2** 106–25
- [40] Liu H, Škereň T, Volodin A, Temst K, Vantomme A and Van Haesendonck C 2015 *Phys. Rev. B* **91** 104403
- [41] Schlömann E 1970 *J. Appl. Phys.* **41** 1617
- [42] Dharmadhikari C V, Ali A O, Suresh N, Phase D M, Chaudhari S M, Ganesan V, Gupta A and Dasannacharya B A 2000 *Solid State Commun.* **114** 377
- [43] Peverini L, Ziegler E, Bigault T and Kozhevnikov I 2007 *Phys. Rev. B* **76** 045411